MODELING OF IDEALITY FACTOR VALUE IN n^+–p–p^+-Si STRUCTURE

O. Ya. Olikh, O. V. Zavhorodnii
Taras Shevchenko National University of Kyiv,
64/13, Volodymyrska St., Kyiv, UA-01601, Ukraine
e-mail: olikh@univ.kiev.ua

(Received 25 August 2020; in final form 19 October 2020; accepted 22 October 2020; published online 01 December 2020)

This paper presents the results of computer simulation of the ideality factor of silicon $n^+ - p - p^+$ structure with iron contamination. The Solar Cells Capacitance Simulator (SCAPS) was the tool used for numerical simulation of these devices. The iron concentration range of $10^{10} - 10^{13}$ cm^{-3}, the acceptor doping level range of $10^{15} - 10^{17}$ cm^{-3}, the temperature range of $290 - 340$ K, and the base thickness range of $150 - 240$ μm were used in the investigation. The double diode model was used to extract the ideality factor. The following cases were considered: (i) uniformly distributed lone interstitial iron atoms; (ii) coexistence of non-uniformly distributed Fe_i and Fe_iB_s. It has been shown that the ideality factor value is determined by a hole occurring on the Fe_i level, a trap location, and an intrinsic recombination contribution. The increase in the base thickness leads to a decrease in n value. The sign of change in the ideality factor after Fe_iB_s dissociation depends on temperature, doping level, and iron concentration.

Key words: ideality factor, silicon, n^+–p–p^+ structure, SCAPS, iron concentration.

DOI: https://doi.org/10.30970/jps.24.4701

I. INTRODUCTION

In literature, there are several models that describe the current–voltage ($I - V$) characteristics of the solar cells (SCs). These models contain some parameters which reflect the processes within the structures and are related to the main characteristics of the photovoltaic conversion. So the single diode model with three parameters has been used to represent the SC static characteristic because of simplicity:

$$I = I_0 \left[\exp\left(-\frac{qV}{nkT}\right) - 1\right] - I_{\rm ph}\,, \qquad (1)$$

were I_0 is the saturation current, n is the diode ideality factor, $I_{\rm ph}$ is the total current generated by a solar cell. The ideality factor value indicates a defect related recombination and directly determines open-circuit magnitude:

$$V_{\rm oc} = \frac{nkT}{q} \ln\left(\frac{I_{\rm ph}}{I_0} + 1\right). \qquad (2)$$

Equation (1) does not take into account a leakage current and a series of losses of load current. Besides, the widely used double diode model is developed by considering the effect of the recombination current loss in the depletion region [1–3]:

$$\begin{aligned} I \;=\; & I_{01}\left[\exp\left(-\frac{q(V - R_{\rm s}I)}{kT}\right) - 1\right] \qquad (3)\\ +\; & I_{02}\left[\exp\left(-\frac{q(V - R_{\rm s}I)}{nkT}\right) - 1\right] + \frac{V - R_{\rm s}I}{R_{\rm sh}} - I_{\rm ph}\,, \end{aligned}$$

where the first term is closely related to the recombination in the quasi-neutral region, the second term describes the overall space charge region (SCR) recombination, $R_{\rm s}$ and $R_{\rm sh}$ are the series and shunt resistance, respectively. In this case the relationship between the ideality factor and SC characteristics is more complicated. Some examples of the relationship between n and open-circuit voltage and the fill factor in the two-diode model can be found in [4]. Typically, the value of the ideality factor ranges from 1 to 2 for real devices and depends on ambient conditions and recombination center parameters, including the concentration of traps [5–9]. This makes the ideality factor an important parameter that can be used to describe the electrical behavior of photovoltaic devices and characterize the recombination in SCs [10].

A major obstacle to the development of such a convenient and express method is the multiparameter relationship between the n value and the concentration of recombination centers. This paper attempts to resolve these difficulties by the simulation of $I - V$ characteristic of silicon solar cells, the determination of ideality factor, and the study of n value depending on simulation parameters. In contrast to the previous paper [11], in this case the n^+–p–p^+-structure, which is closer to the real SC, is under consideration. Additionally, the base thickness is known [12, 13] to affect SC efficiency; therefore, the paper considers the influence of this parameter on the ideality factor value.

The paper focuses on the case when the main recombination centers are the iron related defects. On the one hand, iron atoms are among the most common as well as the most harmful impurities in a silicon solar cell. On the other hand, the Fe_iB_s pairs can be readily dissociated by illumination [13]; the association reaction can take place when exposed in darkness for ten minutes [14]. Such a change in the recombination center state should lead to a change in an ideality factor value, which is easy to obtain experimentally and to use for the SC characterization. Therefore, the paper also pays attention to dependencies of n value change.

II. SIMULATION DETAILS

The calculation presented here uses $n^+ - p - p^+$ structure shown in inset in Fig. 1. Its main parts are the emitter layer with thickness d_n, the base with the hole conductivity and thickness d_p and the p^+ layer with thickness $d_{\rm BSF}$ intended for the back surface field (BSF) creation. BSF-layer is designed to increase the photovoltaic converter efficiency by reducing the losses concerned with the surface recombination and such structure is widely used for both manufacturing of real solar cells and modeling [15–17].

The material of all layers was assumed to be monocrystalline silicon. The temperature dependencies of the bandgap were calculated using the Pässler equations [18]. The bandgap narrowing, thermal carrier velocities, and free carrier effective mass were taken from Yan and Cuevas [19], Green [20], and O'Mara *et al.* [21], respectively. Data from Couderc *et al.* [22] were used to evaluate intrinsic carrier density and density of states effective masses. The temperature dependencies carrier mobilities were described by Klaassen's theory [23, 24].

Uniform doping with phosphorus (the emitter layer, concentration $N_{\rm D}$) and boron (base and BSF–layer, concentrations $N_{\rm A}$ and $N_{\rm BSF}$, respectively) was assumed.

The following recombination processes were taken into account: i) the outside surface recombination with electron and hole velocities 10^3 cm/s; ii) the intrinsic recombination (radiative band-to-band and Auger with coefficients, which depend on temperature and doping level according to Nguyen *et al.* [25] and Altermatt *et al.* [26]); iii) the Shockley–Read–Hall (SRH) recombination.

In the last case, as the base and BSF-layer uniform contaminant, iron is assumed to be in concentration $N_{\rm Fe}$. It is well known that an iron atom is locates in the lone interstitial lattice position in silicon (Fe_i) or interacts with ionized acceptors and combines into a Fe_iB_s pair. The two cases were under consideration. In the first one, uniformly distributed Fe_i with concentration $N_{\rm Fe}$ was assumed. This happens under constant illumination or immediately after its termination. The temperature independent donor level $E_{{\rm Fe}_i} = E_V + 0.394$ eV [27–29] and electron $\sigma_{n,{\rm Fe}} = 3.47 \times 10^{-15} T^{-1.48}$ m^2 and hole $\sigma_{p,{\rm Fe}} = 4.54 \times 10^{-20} \exp\left(-\frac{0.05}{kT}\right)$ m^2 capture cross-sections [30, 31] are associated with Fe_i. In the second one, Fe_i and Fe_iB_s coexisted. They were non-uniformly distributed through the base and BSF-layer. More details are presented elsewhere [11] and representative examples of the calculation are shown in Fig. 2. This happen under dark equilibrium condition. The Fe_iB_s is amphoteric defect and donor level $E^{\rm D}_{\rm FeB} = E_V + 0.10$ eV, $\sigma^{\rm D}_{n,{\rm FeB}} = 4 \times 10^{-17}$ m^2, $\sigma^{\rm D}_{p,{\rm FeB}} = 2 \times 10^{-18}$ m^2 and acceptor level $E^{\rm A}_{\rm FeB} = E_C - 0.26$ eV, $\sigma^{\rm A}_{n,{\rm FeB}} = 5.1 \times 10^{-13} T^{-2.5}$ m^2, $\sigma^{\rm A}_{p,{\rm FeB}} = 3.32 \times 10^{-14} \exp\left(-\frac{0.262}{kT}\right)$ m^2 [14, 27, 28, 30–32] are used in the simulation.

The dark forward dark $I - V$ characteristics were generated by one-dimensional code SCAPS 3.3.08 [33, 34] over a voltage range up to 0.45 V with step 0.01 V. This software is widely applied in modeling various solar cells [15, 16, 35–39], silicon based devices including [15, 16, 39]. The used parameters are listed in Table 1. Thus, the varied parameters were the boron concentrations in the base, iron concentration, base thickness and temperature. Taking into account two defect configuration, 15048 structures were simulated. The examples of $I - V$ curve are shown in Fig. 1.

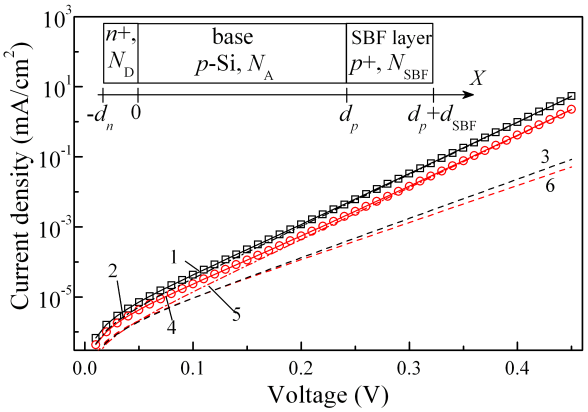

Fig. 1. Simulated I–V characteristic (marks) and its fitting by Eq. (4) (solid lines 1 and 4). The dashed (3, 6) and dotted-dashed (2, 5) lines represent the diffusion and recombination currents, respectively. $N_{\rm A} = 10^{17}$ cm^{-3}, $N_{\rm Fe} = 10^{13}$ cm^{-3}, $T = 340$ K, $d_p = 180$ μm. The results for lone unpaired Fe_i (circles, curves 4–6, red) as well as for Fe_iB_s and Fe_i coexistence (squares, curves 1–3, black) are presented. Inset: Structures, which are used in the simulation

Parameter	Range	Number of values
d_n, μm	0.5	1
d_p, μm	150 – 240	4
$d_{\rm BSF}$, μm	1	1
$N_{\rm D}$, cm^{-3}	10^{19}	1
$N_{\rm A}$, cm^{-3}	$10^{15} - 10^{17}$	9
$N_{\rm BSF}$, cm^{-3}	$5 \cdot 10^{18}$	1
$N_{\rm Fe}$, cm^{-3}	$10^{10} - 10^{13}$	19
T, K	290 – 340	11

Table 1

The simulated $I - V$ characteristics were fitted by the following equation:

$$I = I_{01}\left[\exp\left(-\frac{qV}{kT}\right) - 1\right] + I_{02}\left[\exp\left(-\frac{qV}{nkT}\right) - 1\right]. \quad (4)$$

Equation (4) corresponds to the dark double diode model with both series and shunt resistances neglected. The first diode represents the "ideal" diode, describing the so-called diffusion current characterized by the saturation current I_{01}, and the second diode is the so-called

recombination current, characterized by the saturation current I_{02} and ideality factor n [3]. n, I_{01}, and I_{02} were taken as fitting parameters and the meta–heuristic method IJAVA [40] was used. The representative results of the fitting are shown in Fig. 1 as well.

In the case of lone unpaired Fe_i the following valus were calculated: n_{Fe}^{srh} is the ideality factor if the SRH recombination is taken into account only; n_{Fe} is the ideality factor if both the SRH recombination and the intrinsic recombination are allowed; $\delta n_{Fe}^{srh} = n_{Fe}^{srh} - n_{Fe}$ characterizes the influence of the intrinsic recombination on the ideality factor value. In the case of Fe_iB_s and Fe_i coexistence, the n_{FeB}^{srh}, n_{FeB}, $\delta n_{FeB}^{srh} = n_{FeB}^{srh} - n_{FeB}$ were calculated (indices had the same meaning). Besides, the change of the ideality factor after Fe_iB_s association $\delta n_{Fe-FeB} = n_{Fe} - n_{FeB}$ was calculated as well.

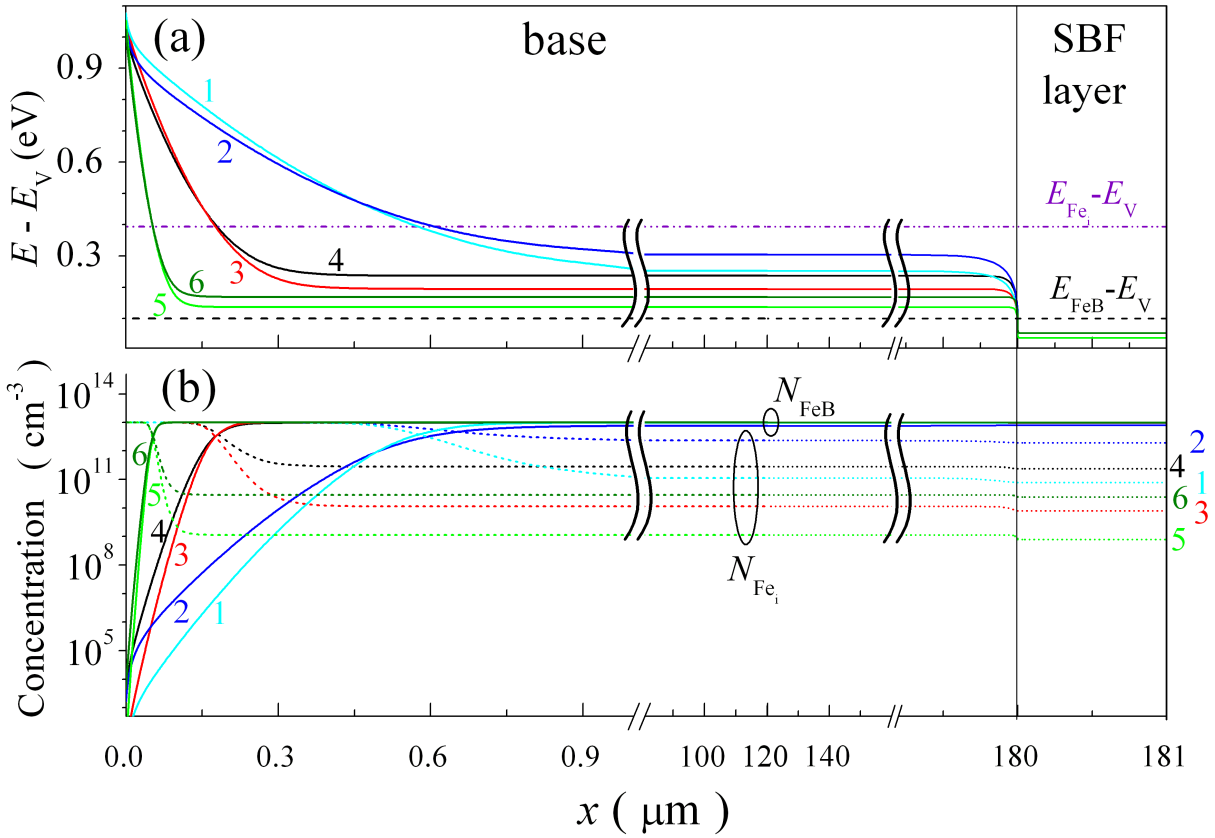

Fig. 2. (Color online). The calculated base and SBF-layer distribution of the Fermi level position (a, solid lines), unpaired interstitial iron concentration (b, dotted lines), and Fe_iB_s pair concentration (b, solid lines) at $V = 0$. N_A, cm^{-3}: 10^{15} (curves 1, 2), 10^{16} (3, 4), 10^{17} (5, 6); T, K: 290 (1, 3, 5), 340 (2, 4, 6); $N_{Fe} = 10^{13}$ cm^{-3}; $d_p = 180$ μm. The positions of Fe_i donor level (dotted-dashed line) and Fe_iB_s donor level (dashed line) are shown in the panel (a) as well

III. RESULTS AND DISCUSSION

Figures. 3–5 show the typical simulated dependencies of the ideality factor value on temperature and both iron and boron concentrations. Note that the δn_{Fe}^{srh} surfaces (number 5, orange) are not shown if they practically coincide with the δn_{FeB}^{srh} surfaces (4, yellow).

One should pay attention to Fig. 2 before a discussion of the obtained dependencies. Firstly, the presented data testify to the primary role of unpaired interstitial iron in recombination even in the case of Fe_iB_s and Fe_i coexistence. In fact, the donor E_{FeB}^{D} level is below the Fermi level and, therefore, the probability of capturing of a non-equilibrium electron is small. Additionally, the ideality factor value above all associated with a SCR recombination and the Fe_i concentration exceeds the Fe_iB_s concentration in the 2/3 thickness of the space charge region. And it is confirmed by the similarity between the dependencies of n_{FeB} (surfaces 1, red) and n_{Fe} (surfaces 2, cyan) in Figs. 3–5. Secondly, the unpaired iron atom concentration can be big enough in the case of Fe_iB_s and Fe_i coexistence as well and it increases with the temperature rise and a decrease in the doping level. For example, the Fe_i concentration in the quasi-neutral region of the base reaches 23 (or 3) percent of N_{Fe} at $T = 340$ K and $N_A = 10^{15}$ cm^{-3} (or 10^{16} cm^{-3}). That is, under these conditions, the concentration of unpaired iron atoms in the dark and $N_{Fe} = 10^{13}$ cm^{-3} is larger than the one under illumination and $N_{Fe} = 10^{11}$ cm^{-3}. Finally, as only ionized iron Fe_i^+ (unlike to neutral iron Fe_i^0) actively takes part in the SRH recombination, these processes efficiently occur at $x \geq 0.6W_p$ (where W_p is the SCR depth). And the area of processes, which determines the ideality factor value, shifts away from the $p - n$ junction with an increase in the doping level.

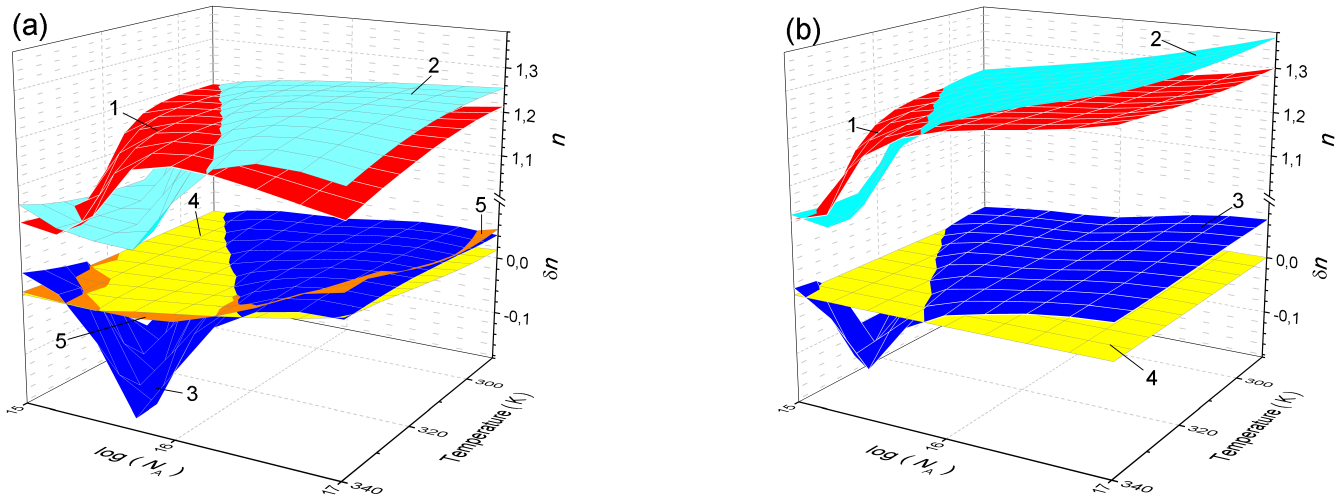

Fig. 3. (Color online). Ideality factor and its change as a function of the temperature and acceptor (boron) concentration. N_{Fe}, cm^{-3}: 10^{10} (a), 10^{13} (b); $d_p = 240$ μm. Surface 1 (red) reflects the n_{FeB} dependance, 2 (cyan) — n_{Fe}, 3 (blue) — $\delta n_{\mathrm{Fe-FeB}}$, 4 (yellow) — $\delta n_{\mathrm{FeB}}^{\mathrm{srh}}$, 5 (orange) — $\delta n_{\mathrm{Fe}}^{\mathrm{srh}}$

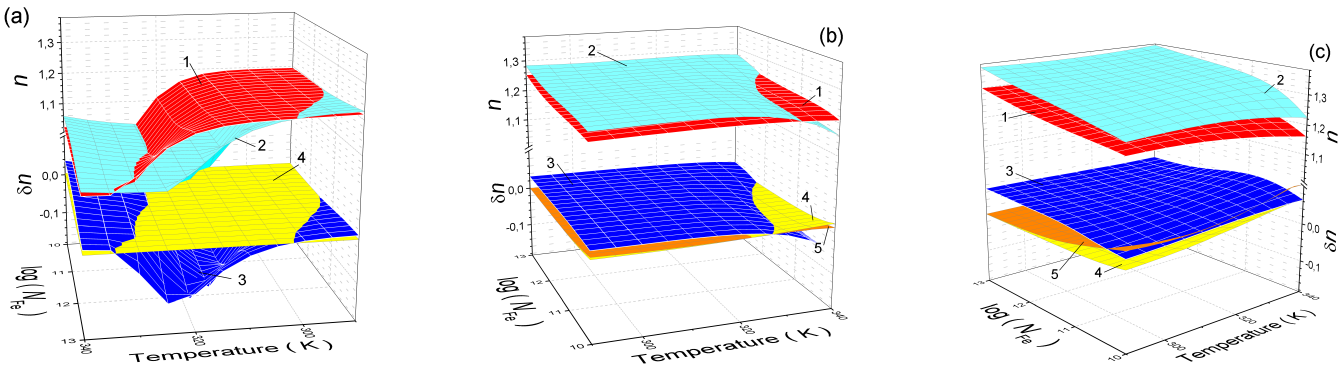

Fig. 4. (Color online). Ideality factor and its change as a function of the temperature and iron concentration. N_{A}, cm^{-3}: 10^{15} (a), 10^{16} (b), 10^{17} (c); $d_p = 150$ μm. Surface numbers are the same as in Fig. 3

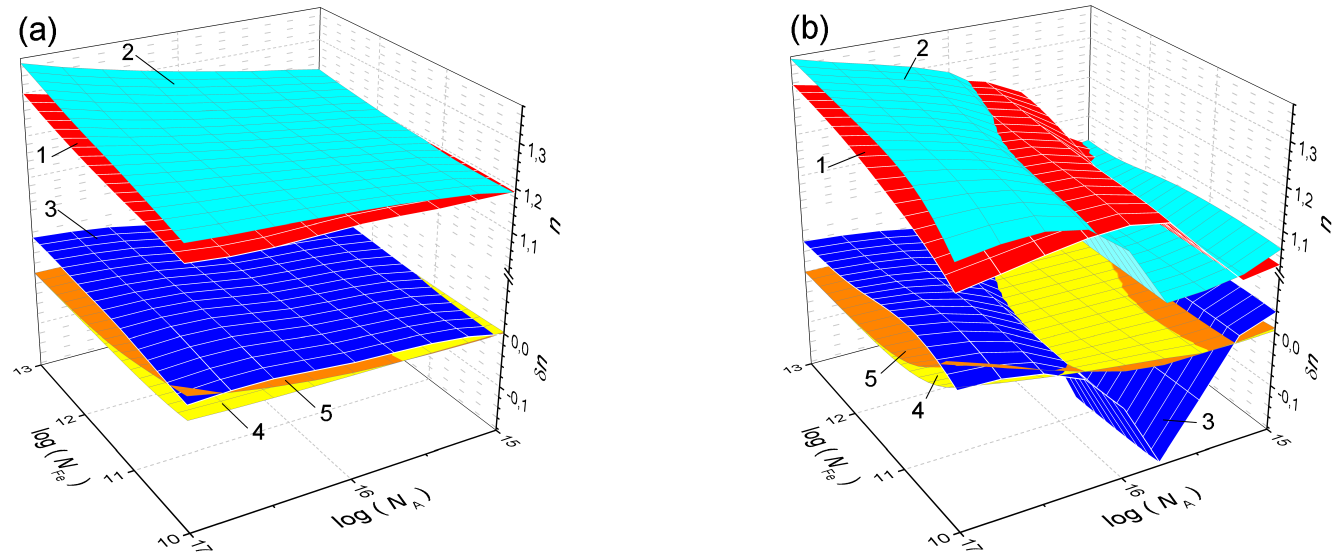

Fig. 5. (Color online). Ideality factor and its change as a function of the acceptor (boron) concentration and iron concentration. T, K: 290 (a), 340 (b); $d_p = 180$ μm. Surface numbers are the same to Fig. 3

Several determinants must be taken into account when analyzing the dependencies of the ideality factor on temperature and the concentration of boron. Namely:

i) the occurrence of a hole on the Fe_i level, which determines the recombination efficiency. Accordingly to the Fermi–Dirac statistics, the probability of a hole occupation in a non-degenerate p-type semiconductor with full acceptor depletion can be expressed as

$$f_p = \frac{1}{1 + \frac{N_V(T)}{N_A} \exp\left(\frac{E_V - E_{Fe_i}}{kT}\right)}. \qquad (5)$$

It has been shown earlier [4] that the $f_p(T, N_A)$ dependence is generally similar to the observed dependence of the ideality factor dependence. In particular, if f_p is close to one (high N_A value and low temperature), this dependence changes slowly, n does not depend on temperature and slowly rises with an increase in the doping level — see Figs. 4(b),(c); 5,(a). If N_A decreases or (and) T increases, the level is filled with an electron in a sufficiently narrow range of arguments, the SRH recombination ceases, and the ideality factor value sharply reduces — Figs. 3, 4(a); 5(b).

ii) the balance of the defect related recombination and the intrinsic recombination. SRH recombination generally causes an increase in the ideality factor value; if the defect related recombination is dominant, the value often reported in publications is $n = 2$. The radiative band-to-band and Auger recombinations are enhanced by the increase in both free charge carrier concentration (doping level) and temperature [25, 26]). In this case, the ideality factor reduces and the values δn_{Fe}^{srh} and δn_{FeB}^{srh} become nonzero. This effect is observed in the corners of surfaces in Figs. 3(a); 4(b),(c); 5.

The change in the impurity iron concentration has almost no effect on the nature of the n dependence on other parameters. However, the N_{Fe} rise is expectedly accompanied by an increase in the ideality factor value (see Figs. 4, 5), which is almost linear with respect to $\ln(N_{Fe})$. An exception is observed only when the level Fe_i is filled with an electron ($n < 1.06$). At the same time, the intrinsic recombination has a greater contribution at a low iron concentration and same other parameters; and a sharp decrease in the ideality factor value is observed in the wake of the low impurity concentration. The striking examples are shown in Figs. 4(b),(c).

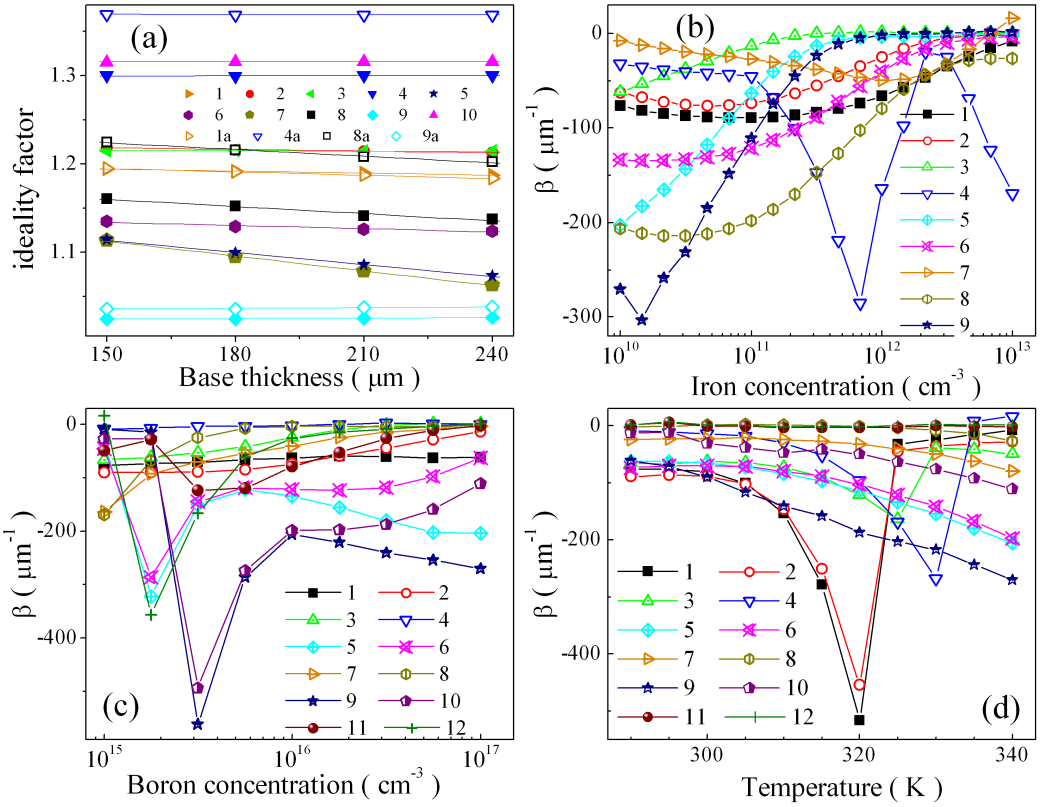

Fig. 6. (a) Typical dependencies of the ideality factor on the base thickness. The results for Fe_iB_s and Fe_i coexistence (curves 1–6, filled marks) as well as for unpaired Fe_i sole (2a, 5a, 6a, empty marks) are presented. T, K: 290 (1, 2, 2a), 320 (3), 340 (4–6, 5a, 6a); N_{Fe}, cm^{-3}: 10^{10} (4, 5, 5a), 10^{12} (3), 10^{13} (1, 2, 2a, 6, 6a); N_A, cm^{-3}: 10^{15} (1, 3, 6, 6a), $3.162 \cdot 10^{15}$ (4), 10^{17} (2, 2a, 5, 5a). The marks are the simulation result, the lines are fitted curves using Eq. (6). (b) Ideality factor thickness coefficient vs iron concentration. T, K: 290 (1, 2), 325 (3), 340 (4–6); N_A, cm^{-3}: 10^{15} (4), 10^{16} (1, 5), 10^{17} (2, 3, 6). (c) Ideality factor thickness coefficient vs boron concentration. T, K: 290 (1, 2), 325 (2–5), 340 (6); N_{Fe}, cm^{-3}: 10^{10} (3, 6), 10^{11} (1, 4), 10^{12} (5), 10^{13} (2). (d) Ideality factor thickness coefficient vs temperature. N_A, cm^{-3}: 10^{15} (1, 2), 10^{16} (3, 4), 10^{17} (5, 6). N_{Fe}, cm^{-3}: 10^{10} (3, 5), 10^{12} (2, 4, 6). Panels (b)–(d) present results in the case of Fe_iB_s and Fe_i coexistence

Taking into account Eq. (3), one can see that the the ideality factor appears in the item connected to the SCR recombination. Therefore, seemingly, n should not depend on the thickness of the n^+–p–p^+ structure base. However, such a dependence is observed (see Fig. 6(a)) and the ideality factor decreases with an increase in thickness. This is evidence that the n value is influenced by processes in the quasi-neutral region as well. The ideality factor changes in a similar way in both lone unpaired Fe_i and Fe_iB_s and Fe_i coexistence cases and described well by a linear dependence

$$n = n_0 - \beta\, d_p\,. \tag{6}$$

where β is the ideality factor thickness coefficient. The maximum effect of thickness is observed at the middle $1.05 < n < 1.25$ value. Figures. 6(b)–(d) show the dependencies of β on the other simulation parameters. One can see that the d_p influence on n generally intensifies with an increase in temperature as well as a decreasing of the concentrations of both boron and iron. The decrease in the relative contribution of SRH recombination due to the electron filling of Fe_i level as well as due to the intensification of the intrinsic recombination causes a decrease in the β module. In addition, Fig. 7 shows the dependencies of the electron diffusion length (L_n) in the base on the concentration of lone unpaired Fe_i, calculated by using SCAPS. Apparently, the influence of the base thickness is observed in the $L_n > d_p$ case only, and this is the reason why $\beta \approx 0$ at $n > 1.3$.

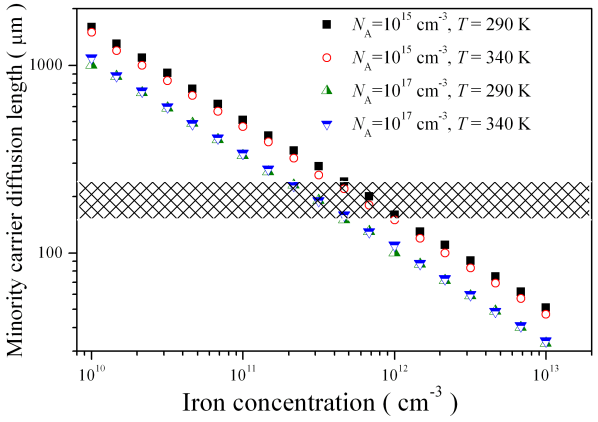

Fig. 7. The calculated dependencies of the electron diffusion length in the structure base in the case of unpaired Fe_i sole. The shaded area represents values of base thickness, were used in the simulation

Also Figs. 3–5 show dependencies of the ideality factor change after the pairing of interstitial iron $\delta n_{\mathrm{Fe-FeB}}$ — see surfaces 3, blue. Since the association reaction leads to the depression of SRH recombination, it was expected that $n_{\mathrm{FeB}} < n_{\mathrm{Fe}}$ and $\delta n_{\mathrm{Fe-FeB}} > 0$ at all the parameters values. The examples of such anticipated dependencies are shown in Figs. 4(b),(c) and 5(a). In this case, $\delta n_{\mathrm{Fe-FeB}}$ increases with an increase in the boron concentration and does not practically depend on temperature and the iron concentration. Exceptions are only observed if the contribution of intrinsic recombination increases and the $\delta n_{\mathrm{Fe-FeB}}$ decreases: see Fig. 4(b),(c) at high temperature and low iron concentration or Fig. 5(a) at high doping level and slight concentration of trap.

However, it turned out that the case of $n_{\mathrm{FeB}} > n_{\mathrm{Fe}}$ is also possible — see Figs. 3, 4(a), 5(b). The regions of negative $\delta n_{\mathrm{Fe-FeB}}$ value are observed in the vicinity of the ideality factor decrease, which is induced by the occupation of Fe_i level. The reason for $n_{\mathrm{FeB}} > n_{\mathrm{Fe}}$ could be the difference in the Fermi level location in the cases of lone unpaired Fe_i and Fe_iB_s and Fe_i coexistence. However, calculations have shown that such difference does not exceed 5×10^{-6} eV and cannot be the cause of the detected effect.

Figure 8 presents the spatial distributions of recombinantly active interstitial iron atoms before and after the pairs formation and transition to the dark equilibrium state. It is evident that the degree of decrease in the Fe_i^+ concentration depends on the distance to the pn–junction. In our opinion, the change in the $N_{Fe_i^+}$ profile is the reason for the rise of the ideality factor resistance to temperature and doping level in the case of Fe_iB_s and Fe_i coexistence. Note that the effect depends on the total iron concentration: the increase in N_{Fe} value leads to the n decay at a higher temperature (Fig. 4(a)) as well as at a lower boron concentration (Fig. 5(b)).

In turn, the $\delta n_{\mathrm{Fe-FeB}}$ the value also depends on the iron concentration in the vicinity of $n_{\mathrm{FeB}} > n_{\mathrm{Fe}}$. As a result, $\delta n_{\mathrm{Fe-FeB}}$, along with n_{Fe} and n_{FeB}, can be used to estimate the impurity concentration by the parameters of $I - V$ characteristic.

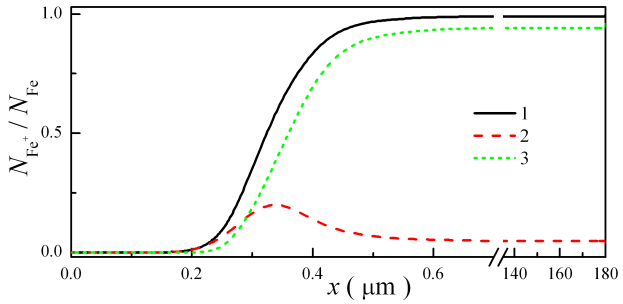

Fig. 8. The distribution of the fraction of positively charged interstitial iron $N_{Fe_i^+}$ to the total impurity number N_{Fe} in the structure base. Curves 1 and 2 correspond to the cases of lone unpaired Fe_i and Fe_iB_s and Fe_i coexistence, respectively. Curve 3 is the difference between 1 and 2. $T = 330$ K, $N_{\mathrm{A}} = 3.162 \times 10^{15}$ cm^{-3}, $d_p = 180$ μm

IV. CONCLUSION

The diode ideality factor of silicon n^+–p–p^+ structure with iron contamination has been studied via computer simulation. The data used in the simulations were the following. The iron concentration ranged from 10^{10} to 10^{13} cm^{-3}, the acceptor doping level — from 10^{15} to 10^{17} cm^{-3}, the temperature — from 290 to 340 K, and the base thickness — from 150 to 240 μm. It has been shown that the temperature and doping level dependencies of

the ideality factor value are mainly determined by a hole occurring on the Fe_i level. The n dependence on iron concentration is a monotonic function. Additionally, not only the concentration of the defect but also its location influences the ideality factor value. The intrinsic recombination causes a decrease in the ideality factor value at a high temperature and doping level as well as at a low iron concentration. It has also been found that the base thickness influences the ideality factor if it exceeds the minority carrier diffusion length. An increase in the base thickness leads to a decrease in n value. The investigation has revealed that the ideality factor in the Fe_iB_s and Fe_i coexistence case can exceed the one in the lone unpaired Fe_i case. The ideality factor change after Fe_iB_s dissociation can be used for the contaminant concentration evaluation.

V. ACKNOWLEDGEMENTS

The work was supported by the National Research Foundation of Ukraine by the state budget finance (project 2020.02/0036 "Development of physical base of both acoustically controlled modification and machine learning-oriented characterization for silicon solar cells").

[1] K. Ishaque, Z. Salam, H. Taheri, Sol. Energy Mater. Sol. Cells **95**, 586 (2011); https://doi.org/10.1016/j.solmat.2010.09.023.

[2] A. J. Bühler, A. Krenzinger, Prog. Photovoltaics Res. Appl. **21**, 884 (2013); https://doi.org/10.1002/pip.2170.

[3] O. Breitenstein, Opto-Electron. Rev. **21**, 259 (2013); https://doi.org/10.2478/s11772-013-0095-5.

[4] O. Olikh, Superlattices Microstruct. **117**, 173 (2018); https://doi.org/10.1016/j.spmi.2018.03.027.

[5] J. Beier, B. Voss, in *Conference Record of the Twenty Third IEEE Photovoltaic Specialists Conference* (1993), p. 321; https://doi.org/10.1109/PVSC.1993.347163.

[6] K. McIntosh, P. Altermatt, G. Heiser, in *16th European Photovoltaic Solar Energy Conference: Proceedings of the International Conference and Exhibition* (Glasgow, 2000), p. 250.

[7] A. Kaminski *et al.*, in *Conference Record of the Twenty Fifth IEEE Photovoltaic Specialists Conference* (1996), p. 573; https://doi.org/10.1109/PVSC.1996.564071.

[8] Z. Hameiri, K. McIntosh, G. Xu, Sol. Energy Mater. Sol. Cells **117**, 251 (2013); https://doi.org/10.1016/j.solmat.2013.05.040.

[9] A. S. H. van der Heide, A. Schonecker, J. H. Bultman, W. C. Sinke, Prog. Photovoltaics Res. Appl. **13**, 3 (2005); https://doi.org/10.1002/pip.556.

[10] L. Duan *et al.*, IEEE J. Photovoltaics **8**, 1701 (2018); https://doi.org/10.1109/JPHOTOV.2018.2870722.

[11] O. Olikh, Superlattices Microstruct. **136**, 106309 (2019); https://doi.org/10.1016/j.spmi.2019.106309.

[12] A. V. Sachenko *et al.*, Tech. Phys. Lett. **44**, 873 (2018); https://doi.org/10.1134/S1063785018100139.

[13] J. Schmidt, Prog. Photovoltaics Res. Appl. **13**, 325 (2005); https://doi.org/10.1002/pip.594.

[14] W. Wijaranakula, J. Electrochem. Soc. **140**, 275 (1993); https://doi.org/10.1149/1.2056102.

[15] E. Hu *et al.*, Renew. Energy **77**, 442 (2015); https://doi.org/10.1016/j.renene.2014.12.049.

[16] A. Hamache, N. Sengouga, A. Meftah, M. Henini, Radiat. Phys. Chem. **123**, 103 (2016); https://doi.org/10.1016/j.radphyschem.2016.02.025.

[17] G. Azzouzi, W. Tazibt, Energy Procedia **41**, 40 (2013); https://doi.org/10.1016/j.egypro.2013.09.005.

[18] R. Pässler, Phys. Rev. B **66**, 085201 (2002); https://doi.org/10.1103/PhysRevB.66.085201.

[19] D. Yan, A. Cuevas, J. Appl. Phys. **116**, 194505 (2014); https://doi.org/10.1063/1.4902066.

[20] M. A. Green, J. Appl. Phys. **67**, 2944 (1990); https://doi.org/10.1063/1.345414.

[21] W. O'Mara, R. Herring, L. Hant, *Handbook of Semiconductor Silicon Technology* (Noyes Publications, New Jersey, 1990).

[22] R. Couderc, M. Amara, M. Lemiti, J. Appl. Phys. **115**, 093705 (2014); https://doi.org/10.1063/1.4867776.

[23] D. Klaassen, Solid-State Electron. **35**, 953 (1992); https://doi.org/10.1016/0038-1101(92)90325-7.

[24] R. Hull, *Properties of Crystalline Silicon* (Institution of Engineering and Technology, London, 1999).

[25] H. T. Nguyen, S. C. Baker-Finch, D. Macdonald, Appl. Phys. Lett. **104**, 112105 (2014); https://doi.org/10.1063/1.4869295.

[26] P. P. Altermatt, J. Schmidt, G. Heiser, A. G. Aberle, J. Appl. Phys. **82**, 4938 (1997); https://doi.org/10.1063/1.366360.

[27] S. Rein, S. W. Glunz, J. Appl. Phys. **98**, 113711 (2005); https://doi.org/10.1063/1.2106017.

[28] J. D. Murphy, K. Bothe, M. Olmo, V. V. Voronkov, R. J. Falster, J. Appl. Phys. **110**, 053713 (2011); https://doi.org/10.1063/1.3632067.

[29] H. Kohno, H. Hieslmair, A. A. Istratov, E. R. Weber, Appl. Phys. Lett. **76**, 2734 (2000); https://doi.org/10.1063/1.126459.

[30] F. E. Rougieux, C. Sun, D. Macdonald, Sol. Energy Mater. Sol. Cells **187**, 263 (2018); https://doi.org/10.1016/j.solmat.2018.07.029.

[31] B. B. Paudyal, K. R. McIntosh, D. H. Macdonald, in *34th IEEE Photovoltaic Specialists Conference (PVSC)* (2009), p. 1588.

[32] A. A. Istratov, H. Hieslmair, E. Weber, Appl. Phys. A Mater. Sci. Proc. **69**, 13 (1999); https://doi.org/10.1007/s003390050968.

[33] M. Burgelman, P. Nollet, S. Degrave, Thin Solid Films **361–362**, 527 (2000); https://doi.org/10.1016/S0040-6090(99)00825-1.

[34] K. Decock, S. Khelifi, M. Burgelman, Thin Solid Films **519**, 7481 (2011); https://doi.org/10.1016/j.tsf.2010.12.039.

[35] M. Cappelletti, G. Casas, A. Cédola, E. Peltzer y Blancá, B. M. Soucase, Superlattices Microstruct. **123**, 338 (2018); https://doi.org/10.1016/j.spmi.2018.09.023.

[36] M. Mostefaoui, H. Mazari, S. Khelifi, A. Bouraiou, R. Dabou, Energy Procedia **74**, 736 (2015); https://doi.org/10.1016/j.egypro.2015.07.809.

[37] C.-H. Huang, W.-J. Chuang, Vacuum **118**, 32 (2015); https://doi.org/10.1016/j.vacuum.2015.03.008.
[38] F. Azri, A. Meftah, N. Sengouga, A. Meftah, Solar Energy **181**, 372 (2019); https://doi.org/10.1016/j.solener.2019.02.017.
[39] B. Zhao, J. Zhou, Y. Chen, Physica B Cond. Mat. **405**, 3834 (2010); https://doi.org/10.1016/j.physb.2010.06.012.
[40] K. Yu, J. Liang, B. Qu, X. Chen, H. Wang, Energy Convers. Manag. **150**, 742 (2017); https://doi.org/10.1016/j.enconman.2017.08.063.

МОДЕЛЮВАННЯ ФАКТОРА НЕІДЕАЛЬНОСТІ В n^+–p–p^+-Si-СТРУКТУРАХ

О. Я. Оліх, О. В. Завгородній
Київський національний університет імені Тараса Шевченка,
вул. Володимирська, 64/13, Київ, 01601, Україна

У цій роботі подано результати моделювання величини фактора неідеальності кремнієвих $n^+ - p - p^+$-структур. При цьому вважалося, що основні рекомбінаційні центри в базі структури пов'язані з домішковими атомами заліза. Для моделювання вольт-амперних характеристик таких структур використано Solar Cells Capacitance Simulator (SCAPS). При цьому додатково враховували температурні залежності параметрів як матеріалу, так і дефектів. Під час розрахунків варіювалися величини рівня леґування ($10^{15} \div 10^{17}$ см$^{-3}$ атомів бору) та товщини ($150 \div 240$ мкм) бази, температура ($290 \div 340$ K) та концентрації домішки заліза ($10^{10} \div 10^{13}$ см$^{-3}$). Окремо розглядали випадки, коли всі атоми заліза перебували в міжвузольному положенні Fe_i та коли переважна частина з них утворювала пари з леґуючою домішкою Fe_iB_s. Останній випадок відповідає стану рівноваги за відсутності освітлення і при цьому співвідношення між концентраціями Fe_i та Fe_iB_s визначалося положенням рівня Фермі та температурою. Визначення величини фактора неідеальності (n) відбувалося апроксимацією (з використанням метаеврістичного методу IJAVA) отриманих вольт-амперних характеристик.

Показано, що навіть за наявності Fe_iB_s основну роль у формуванні величини n відіграють процеси рекомбінації за участю рівнів, пов'язаних з Fe_i. Залежності n від температури та рівня леґування визначають, насамперед, заселеністю рівня Fe_i. Коли підсилюється відносний внесок процесів власної рекомбінації (високі температури та рівень леґування, низькі концентрації домішки), відбувається зменшення фактора неідеальності. На величину n, окрім концентрації дефектів, впливає також їх просторове розташування щодо $p - n$-переходу. Зі збільшенням товщини бази структури (коли вона перевищує довжину дифузії неосновних носіїв та коли переважає рекомбінація Шоклі–Ріда–Голла) відбувається незначне зменшення фактора неідеальності. Показано, що можуть реалізуватися випадки, коли n після розпаду Fe_iB_s зменшується. Запропоновано, що зміна фактора неідеальності після розпаду Fe_iB_s, поряд з абсолютним значенням n, може бути використана для оцінки концентрації домішок.

Ключові слова: фактор неідеальності, кремній, n^+–p–p^+-структура, SCAPS, концентрація заліза.